Circular RNA hsa-circ-0005283 enhances trophoblast cell migration and invasion and suppresses trophoblast apoptosis by regulating miR-370-3p/CDC25B axis

Jilong Yao (dryaojilong369@163.com)
Southern Medical University
Zhuomin Huang
Southern Medical University
Litong Zhu
Southern Medical University
Depeng Zhao
Southern Medical University
Quanfu Zhang
Jinan University

Research Article

Keywords: circular RNAs, fetal growth restriction, hsa-circ-0005238, trophoblast, miR-370-3p

Posted Date: March 7th, 2022

DOI: https://doi.org/10.21203/rs.3.rs-1327549/v1

Abstract

Background: A large body of evidence shows that insufficient trophoblast invasion and proliferation contributes to the pathogenesis of fetal growth restriction (FGR). Circular RNAs (circRNAs) were recently recognized to have a part in regulating the trophoblast function. We aim to elucidate the role of circRNAs underlying the development of FGR.

Methods: The expression of circRNAs in placenta tissues with and without FGR were identified using next generation sequencing (NGS). In vitro experiments including transfection, qRT-PCR, western blotting, immunofluorescence staining, dual-luciferase assays, cell invasion and migration assays were performed.

Results: We found that 18 circRNAs were differentially expressed between the FGR placentas and uncomplicated pregnancies, while the expression of hsa-circ-0005238 was significantly lower in the FGR placentas. Our in vitro experiments further showed that hsa-circ-0005238 inhibited apoptosis and promoted migration, invasion of trophoblast cell lines. The hsa-miR-370-3p was identified as a direct target of hsa-circ-0005238. Mechanistically, hsa-miR-370-3p inhibits invasion and migration of trophoblast cells by suppressing the expression of CDC25B.

Conclusions: The findings of the present study suggest that hsa-circ-0005238 play an important role in the pathogenesis of FGR by suppressing trophoblast cell invasion and migration through sponging hsa-miR-370-3p, which may provide new insight into therapeutic target for FGR.

Background

Fetal growth restriction (FGR) is a pathological condition in which the estimated fetal weight or abdominal circumference is less than the 10th percentile for gestational age[12]. FGR is the significant risk factor of neonatal death, accounting for 5–10% of newborns, increasing the risk for mortality by two-fold compared to those with normal fetal growth[25, 26]. Moreover, growth restriction of fetuses also contributes to the development of diabetes, cardiovascular disease and stroke in adulthood[7–9].

The known risk factors of FGR include maternal complications (such as pre-eclampsia and type 2 diabetes, and connective tissue disorders) and fetal complications (such as twin pregnancies, aneuploidy), accounting for 70% of FGR cases[24, 25]. The etiology of FGR is complex, despite uterine–placental perfusion is considered as a major cause[12], mechanism underlying the pathogenesis of FGR remains unclear.

It has now been recognized that dysregulation of non-coding RNAs (ncRNAs) is association with the initiation and progression of many diseases[4, 6, 10]. CircRNAs are single-stranded RNAs, which can form covalently closed loops and have multiple function, including direct interactions with RNA-binding proteins, modulation of parental gene expression and sponging miRNAs[18, 27]. CircRNA studies are mainly lying in the field of cancer and other chronic diseases, and little is known about placental transcriptome,

especially in disease settings. Recently Gong et al.[13] analyzed human the transcriptome from 302 human placentas, including 56 cases of FGR, and characterized several dysregulated transcripts relating to FGR. They also found some placental circular RNAs may potential be diagnostic or therapeutic targets of FGR. Nevertheless, the role of circRNAs in FGR is still unclear.

In the current study, we first used next generation sequencing (NGS) to investigate the transcriptome profiles of placentas from FGR and healthy pregnant women. Then, we verified the differentially expressed circRNAs using quantitative real-time polymerase chain reaction (qRT-PCR). Furthermore, we investigated the role of identified hsa-circ-0005238 via regulation of the miR-370-3p/CDC25B axis in the biological process in cultured trophoblast cells. Hence, the purpose of this study was to add to the mechanism of pathogenesis in FGR.

Materials And Methods

Tissue samples

Forty placentae from pregnant women with FGR and forty placentae from normal pregnant women were included in this study. The participants of both groups had normal blood routine, normal liver and kidney function, normal blood pressure, and normal blood glucose concentration. Three placenta samples of FGR and three of normal placenta were collected for circRNA next generation sequencing (NGS). All samples were for qRT-PCR assay. Each placental tissue was divided into four parts. One part of the placental tissues was immersed in RNA protective solution (Sangon Biotech, Shanghai, China) immediately after collection, then frozen in liquid nitrogen for use later. This study was approved by the Medical Ethics Committee of Shenzhen Maternity and Child Healthcare Hospital.

RNA sequencing

Three placental samples of both groups (FGR and normal control) were used for RNA sequencing. Total RNA from tissue samples was extracted using TRIzol reagent (Invitrogen). RNA integrity was analyzed by the Agilent Bioanalyzer 2100 system (Agilent Technologies, CA, USA). Total RNA samples were used in subsequent experiments if the following requirements were met: RNA integrity number (RIN) ≥ 7.0, $OD_{260/280}$ ≥1.7 and 28S:18S ratio ≥ 1.5:1. Library construction and RNA sequencing service were provided by CapitalBio Co., Ltd. (Beijing, China). A total amount of 5 μg RNA per sample was used. Base calling was performed on the original image files of Illumina high-throughput sequencing, which was converted into raw data. FastQC software was applied to evaluate the sequencing quality of raw data of and the content of A, T, C, and G bases in the sequencing data. Low quality data were filtered using fastp software. The clean reads with high quality were then aligned to the human reference genome (GRCh38/hg38) using Tophat2 software with default parameters. The sequencing data that cannot aligned to reference genome directly were subjected to the subsequent circRNA analysis by recognition of the reverse splicing event using Find_circ and CIRCexplorer2 software[34]. SRPBM software was used to analyze the different expression of circRNAs[16]. Quantile normalization was conducted using customized

R software package. circRNAs having |log2FC|≥1 and p-values ≤ 0.05 were determined as being significantly differentially expressed by Limma package of R software and edge package of R software. Function annotation and pathway enrichment analyses for the host genes of differentially expressed circRNAs were performed with KOBAS[2].

RNA extraction and quantitative reverse transcription PCR (RT-qPCR) assay

Total RNA from placental tissues or trophoblast cells was isolated with TRIzol reagent (Invitrogen). The ImProm-IITM Reverse Transcription System (Promega, Madison, WI, United States) was adopted to produce cDNA from RNA. Reverse transcription used random primers to detect circRNAs. Quantitative RT-PCR (RT-qPCR) assay was conducted in the SYBR GREEN qPCR Super Mix (Promega, United States). The expression of GAPDH was opted as the internal control for target circRNA and mRNA. The expression of U6 functioned as the internal control for miRNA. All assays included three independent experiments. The relative expression of RNA was quantified using the $2^{-\Delta\Delta Ct}$ values. The primers for RT-qPCR assay were present in Table 1.

Table 1
Primer of circRNAs

circRNA	sequence	size of product
hsa_circ_0006427-F	GCCAGGCTGTGACTTTTGAA	156bp
hsa_circ_0006427-R	TAACCTTGTGATCTGCCAGGA	
hsa_circ_0103279-F	AGTGCTAAAAAGGAGAAATTGTCG	196bp
hsa_circ_0103279-R	AAAGGGACATCGTGTTCACC	
hsa_circ_0005238-F	AGTTTTGCAGTCGAGGAGTT	143bp
hsa_circ_0005238-R	GCAAGTTGTGCATCCCATTC	
hsa_circ_0035897-F	TCCTCAGTGCTTGGTCCATC	150bp
hsa_circ_0035897-R	TTAGTGGCGTCACAGAATCAG	
hsa_circ_0072697-F	AGGCTTATCCAACCAGCGTA	201bp
hsa_circ_0072697-R	TGCATGTAACTGCGCTCATA	
hsa_circ_0000972-F	GCTGATTTTTCAGGGTCAACT	131bp
hsa_circ_0000972-R	GCCCAAAAGGGTAGCAACTA	
hsa_circ_0088213-F	TCGCCAGAATGCACTGTTAC	171bp
hsa_circ_0088213-R	CATCCAAGTAGGCTCTTTCAA	
hsa_circ_0084748-F	TCTGGCATCCATTTGCGTTA	235bp
hsa_circ_0084748-R	CGCCACTAGCATGTAGAAGAA	
hsa_circ_0137008-F	TGGCAGTCTCACATTGAAGG	316bp
hsa_circ_0137008-R	CCTTCCAAGGGAACATCTGTG	
hsa_circ_0006222-F	ACAGCAGAAGAGATGATATTGCT	136bp
hsa_circ_0006222-R	TCAGAAAGCGAAAGCTGGTC	
hsa_circ_0005939-F	ACCCTTCTCAATCATCAGCAA	167bp
hsa_circ_0005939-R	TTGTTCATCTGATTTTCTCTTGT	
hsa_circ_0005286-F	CATCAGAACAGAGTGGTGCT	147bp
hsa_circ_0005286-R	GGCACAATAGTTGTAGAGGCA	
hsa_circ_0007440-F	ACATGGGCAATGTGATTTGATG	216bp
hsa_circ_0007440-R	TTGCCAGCATTCCTCAACTT	

circRNA	sequence	size of product
hsa_circ_0005078-F	AGATGTTCTTGCACAGGGTG	137bp
hsa_circ_0005078-R	GACAGGTTGTCTGTATACTGCT	
hsa_circ_0003288-F	ACAGGTTGGTCCTACAGC	168bp
hsa_circ_0003288-R	AGTTGGCCTCGTGGCATT	
hsa_circ_0002590-F	CTCCGCACGGTATTATTG	157bp
hsa_circ_0002590-R	GTCCTGCTATTTCTCCTCTT	
hsa_circ_0086190-F	GACACGCCCGCACAAAGA	108bp
hsa_circ_0086190-R	GCAATGCTGGCAAACAGG	
hsa_circ_0005204-F hsa_circ_0005204-R	GTTCTACTCCTCCGTCTTCG CTCCAGCATCTTGTTCACAG	254bp

Cell Culture and Transfection

Human extra-villous trophoblast cell line of HTR-8/SVneo from the American Type Culture Collection (ATCC) was employed for in vitro experiments. The HTR-8/SVneo cells were cultured in RPMI 1640 medium (Gibco, Carlsbad, CA, United States), added with 10% fetal bovine serum (Gibco, Carlsbad, CA, United States) and penicillin/streptomycin (1%, Solarbio, Beijing, China). HTR-8/SVneo cells were incubated at 37˚C in humidified air with 5% CO_2.

Hsa-circ-0005238, located at chr21:17205666–17214859, was cloned into thepLCD5H-ciR plasmid between EcoRI and BamHI sites (Guangzhou Geneseed Biotech Co., Ltd., China), by DNA synthesis in vitro, to construct the hsa-circ-0005238 overexpression vector (ov-circ-0005238). Negative control (NC) was empty pLCD5H-ciRplasmid. Small interfering RNA (siRNA) binding hsa-circ-0005238 was synthesized to knockdown hsa-circ-0005238. The above vector or siRNAs was transfected into the HTR-8/SVneo cells with dosage of 1 mg/per well or concentration of 50 nM using Lipofectamine TM 2000 Reagent (Invitrogen, Carlsbad, CA, United States). MiR-370-3p mimic and inhibitor as well as their matched negative controls (miR-NC and miR-NC-inhibitor) were obtained from the GenePharma Co. (Shanghai, China). Lipofectamine 2000 reagent (Invitrogen) was used for cellular transfection according to the manufacturer's protocol. After transfection, cells were collected for the subsequent assays.

Flow cytometry analysis for cell apoptosis

The flow cytometry assay for cell apoptosis was performed according to the standard protocols of Annexin V-FITC/PIApoptosis Detection Kit (KeyGEN Biotech, Nanjing, China). The HTR-8/SVneo cells were harvested 48 hours after transfection and further incubated on ice for 5 min in the dark with a mixture of 5 ml Annexin V-FITC and 5 ml propidium iodide. BD FACSCalibur flow cytometer was used to analyze the apoptosis of HTR-8/SVneo cells. Cell apoptosis index was demonstrated in the FlowJo software version

8 (FlowJo, Ashland, OR, United States). The early and late (+) apoptotic cells were stained by AnnexinV-FITC^{+}/PI^{-} or AnnexinV-FITC^{+}/PI^{+}, respectively. The proportion was calculated by the number of early or late cells over the total number of all apoptotic cells to evaluate the cellular apoptosis. Each experiment was performed in triplicates.

Cell Migration and Invasion Assay

24 hours post transfection, HTR-8/SVneo cells were incubated in serum-free medium for starvation of24h. Migration assay was performed in the Transwell chambers (Corning, Steuben County, NY, United States) with 24 wells and 8 μm pores. The invasion experiments were done in Transwell chambers with Matrigel (BD Biosciences, Bedford, MA, United States). HTR-8/SVneo cells moving to the lower membrane surface were counted.

Bioinformatic Analysis

All the information of circRNAs was acquired from circBase (http://www.circbase.org/). Target miRNAs of hsa-circ-0005283 or hsa-miR-370-3p were searched the TargetScan databases (http://www.targetscan.org/vert_71/).

Dual Luciferase Activity Assay

Fragments of wild-type hsa-circ-0005283 including the binding sequences of hsa-miR-370-3p were amplified and cloned into the psi-CHECK-2 vector (Promega) to assemble the recombinant luciferase reporter plasmid. This plamid was termed as ‘wt-circ-0005238’. In this recombinant plasmid, the binding sequences of hsa-miR-370-3p were mutated via site-directed mutagenesis using one-step overlap extension PCR. This mutated plasmid was termed as ‘mut-circ-0005283’. HTR-8/SVneo cells were further transfected with 100 ng recombinant plasmid and 50 nM of hsa-miR-370-3p mimic or miR-NC on 24-well plates. Forty-eight hours after co-transfection, Dual-Luciferase Reporter Assay System (Promega) was adopted to measure the Firefly and Renilla luciferase activities according to the manufacturer’s instructions. Relative luciferase activity was expressed as the ratio of Renilla and Firefly luciferase activities (R/F). Each experiment was performed in triplicates.

Anti-AGO2 RNA Immunoprecipitation (RIP) Assay

The RIP assay was performed using the Magna RIP RNA-Binding Protein Immunoprecipitation Kit instructions (Millipore, Bedford, MA, United States). First, according to the manufacturer’s instructions, HTR-8/SVneo cells transfected with hsa-miR-370-3p mimic or miR-NC were prepared and then were lysed in polysome lysis buffer with protease inhibitor cocktail. Before immunoprecipitation, a positive control in the RIP assay, called "input," was obtained from a portion of the cell lysate. Following that, 100 μL of cell lysate were treated overnight at 4°C with magnetic bead-antibody (IgG or Ago2). Finally the RNA was extracted and purified. The levels of hsa-circ-0005283 in purified RNA were detected by RT-qPCR. Each experiment was performed in triplicates.

Western Blot Analysis

Protein concentrations were determined by the Bio-Rad Protein Assay Kit (Bio-Rad Laboratories, Hercules, CA, United States). To separate the proteins, sodium dodecyl sulfate-polyacrylamide gel electrophoresis was used. After separation, the proteins were then transferred onto a polyvinylidene fluoride membrane. The membranes were then treated overnight at 4°C with primary antibodies (CDC25B, 1:1,000. Abcam, Cambridge, MA, United States). The membranes were then washed and incubated for 2 hours at room temperature with a secondary antibody (anti-rabbit IgG, HRP-linked Antibody, 1:5,000). Lastly, increased chemiluminescence (Pierce, Rockford, IL,

United States) was used to see the bands on the membranes, and the signals were subjected to X-ray. Each experiment was performed in triplicates. The ratio of the target protein densitometric value to the GAPDH densitometric value was used to measure relative protein expression.

Statistical Analysis

Data were displayed as mean ± standard deviation (SD) The t-tests or non-parametric tests were employed to analyze the data of normal or skewed distribution A statistical significance was reached if $P < 0.05$. SPSS version 20.0 (IBM Corp, Armonk, NY, United States) and GraphPad Prism version 5.0 (GraphPad Software, San Diego, CA, United States) were used to analyze the data.

Results

The clinical characteristics of FGR and healthy pregnant women

As shown in Table 2, there was no significant difference between the maternal age, height, weight, BMI, and week of delivery in the FGR group and the matched normal control group ($P > 0.05$), while the birth weight of the fetus, fetal length, fetal head circumference, and fetal thoracic circumference in the FGR group were significantly lower than those in the matched normal control group ($P < 0.001$).

Table 2
Summary of clinical characteristics

Items	FGR	Control	*P* value
Number	40	40	
Age(y)	29.08 ± 3.25	28.35 ± 3.83	0.847
Height(cm)	159.59 ± 5.26	159.81 ± 5.13	0.364
Weight(Kg)	60.70 ± 9.04	63.356 ± 6.27	0.131
BMI	23.78 ± 3.10	24.77 ± 1.69	0.080
Week of delivery	37.55 ± 0.71	37.75 ± 0.67	0.200
Birth weight of the fetus(g)	2285.50 ± 192.83	3254.50 ± 289.88	*p < 0.001*
Fetal length(cm)	46.75 ± 2.33	50.10 ± 0.71	*p < 0.001*
Fetal head circumference(cm)	32.35 ± 1.10	34.13 ± 0.69	*p < 0.001*
Fetal thoracic circumference(cm)	31.35 ± 1.10	33.13 ± 0.69	*p < 0.001*

Differentially expressed circRNAs and cluster analysis

NGS of three placenta samples from each group was performed to explore the role of placenta abnormalities in FGR pathogenesis. RNA sequencing data analyzed in the article have been deposited into CNGB Sequence Archive (CNSA)[14] of China National GeneBank DataBase (CNGBdb)[3] (https://db.cngb.org/cnsa/) with accession number CNP 0002703. A total of 3,069 circRNAs were differentially expressed between the two groups. After applying a criterion of $P \leq 0.05$ and $|\log2FC| \geq 1$, 19 circRNAs were identified. Among these 19 circRNAs, 9 were upregulated and 10 were downregulated, as demonstrated by heatmap (Fig. 1A) and volcano plot (Fig. 1B). Due to the failure in synthesizing primers of some identified circRNA, the left 8 up-regulated and 10 down-regulated circRNAs in the FGR group were shown in Table 3.

Table 3
Differentially expressed circRNAs

up-regulation circRNAs		down-regulation circRNAs	
circRNA	logFC	circRNA	logFC
hsa-circ-0072697	6.26	hsa-circ-0005078	-5.76
hsa-circ-0005286	5.34	hsa-circ-0084748	-5.57
hsa-circ-0003288	5.38	hsa-circ-0007440	-5.42
hsa-circ-0103279	5.18	hsa-circ-0035897	-5.28
hsa-circ-0005939	5.10	hsa-circ-0005204	-5.56
hsa-circ-0006427	5.06	hsa-circ-0137008	-5.11
hsa-circ-0006222	5.10	hsa-circ-0005238	-5.07
hsa-circ-0088213	2.54	hsa-circ-0086190	-5.29
		hsa-circ-0002590	-4.98
		hsa-circ-0000972	-5.31

GO and KEGG enrichment of differentially expressed circRNAs

We further performed GO and KEGG enrichment analysis to gain further insights into the biological processes, which these differentially expressed circRNAs in FGR could act on. The top 5 significantly enriched biological processes by GO enrichment were primary metabolic process, organic substance metabolic process, metabolic process, cellular metabolic process, cellular macromolecule metabolic process (Fig. 2A). The top 5 enriched by KEGG were pathways in cancer, thyroid hormone signaling pathway, longevity regulating pathway, PI3K-Akt signaling pathway, phosphatidyl inositol signaling system (Fig. 2B).

Validation of the circRNAs expression levels in FGR tissue

Placental samples from 40 FGR women and 40 healthy pregnant women were obtained for validation of the differentiated expression of circRNAs. The relative expression of the 18 identified CircRNAs were consistent with the NGS data (Fig. 3A). Then we checked for the specificity of the qRT-PCR products by melting curve analysis and agarose gel electrophoresis (Fig. 3B). Among the 18 circRNAs, hsa-circ-0005238, located at chr21:17205666–17214859. was the most influenced one. The position of the splice junctions was verified by sequencing analysis of the hsa-circ-0005238 fragment via qRT-PCR (Fig. 3C).

Hsa-circ-0005238 suppressed apoptosis and enhanced migration, invasion in trophoblast cells

We further investigated the function of hsa-circ-0005238 by overexpressing or silencing hsa-circ-0005238 in trophoblast cells. After transfection with ov-circ-0005238, the expression level of hsa-circ-0005238 increased in HTR-8 cells compared with NC group (Fig. 4A). Simultaneously, after transfection with si-circ-0005238, the expression level of hsa-circ-0005238 decreased in HTR-8 cells compared with si-NC group (Fig. 4B).

The role of hsa-circ-0005238 in cell apoptosis was detected by flow cytometry. As shown in Fig. 4C and 4D, overexpression of hsa-circ-0005238 significantly inhibited both early and late apoptosis in HTR-8 cells, while silence of hsa-circ-0005238 significantly promoted both early and late apoptosis compared with the control.

Furthermore, the role of hsa-circ-0005238 in cell migration was studied using Transwell assay. As shown in Fig. 4E and 4F, ov-circ-0005238 group had more cells migrated to the bottom chamber, but the si-circ-0005238 group, by contrast, had less cells than the si-NC group. Besides, more cells invaded through the Matrigel in the ov-circ-0005238 group than in the NC group and less in the si-circ-0005238 group than in the si-NC group.

Hsa-circ-0005238 Targeted hsa-miR-370-3p

Follow online bioinformatics prediction by TargetScan, we screened 4 microRNA which had high context + score percentile as candidate microRNA– miR-6893-3p, miR-370-3p, miR-3065-5p, miR-5585-3p. We first investigated the expression of these 4 microRNAs in ov-circ-0005283, ov-NC, si-circ-0005283 and si-NC HTR-8 cells. We found that hsa-miR-370-3p expression was significantly depressed in the ov-circ-0005283 group than in the ov-NC group ($P = 0.002$), while its expression was risen in the si- circ-0005283 group than in the si-NC group ($P = 0.003$) (Fig. 5A), indicating that hsa-circ-0005283 might be a miR-370-3p sponge. Then, we verified the expression of hsa-miR-370-3p in 40 FGR and 40 normal placental tissues. The results indicated that hsa-miR-370-3p expression was significantly higher in the FGR placental tissues (Fig. 5B).

Moreover, dual luciferase activity assay was to confirm the binding of hsa-miR-370-3p to linear hsa-circ-0005283. As shown in Fig. 6A, we predicted the binding site of hsa-miR-370-3p on wild type hsa-circ-0005283. Figure 6A also showed the sequence of the mutant hsa-circ-0005283. Figure 6B showed the results of dual luciferase activity assay. After hsa-miR-370-3p mimic + wt-circ-0005238 transfection, relative luciferase activity was lower than after NC transfection, while relative luciferase activity was higher after hsa-miR-370-3p inhibitor + wt-circ-0005238 transfection. However, the mut-circ-0005238 transfection group failed to get the same results. On the other hand, an anti-AGO2 RIP assay was performed to further confirm whether hsa-miR-370-3p binds to hsa-circ-0005283. As shown in Fig. 6C, anti-AGO2 RIP assay results showed that hsa-circ-0005283 levels were higher in the RIP product of miR-370-3p -transfected cells than those in the miR-NC-transfected cells. To summarize what had been mentioned above, hsa-miR-370-3p could bound to the endogenous hsa-circ-0005283 in HTR-8 cells.

Hsa-miR-370-3p Overexpression Reversed the Effect of hsa-circ-0005283 Overexpression in HTR-8 Cells

To further verify the above findings, hsa-circ-0005283 overexpression plasmid and hsa-miR-370-3p mimics were transfected at the same time into HTR-8 cells. On one hand, as shown in Fig. 7A, the cells number of the ov-circ-0005283 + miR-370-3p group migrating to the bottom chamber was lower than that in the ov-circ-0005283 + miR-NC group. Meanwhile, cells invasion showed the similar results as migration. In the ov-circ-0005283 + miR-370-3p group, On the other hand, the percentage of apoptotic cells was higher than in the ov-circ-0005283 + miR-NC group as shown in Fig. 7B. Furthermore, there were no significantly differences between the ov-circ-0005283 + miR-370-3p group and NC + miR-NC group in the migration, invasion or apoptotic assays. All these results above suggested that hsa-miR-370-3p overexpression reversed hsa-circ-0005283 overexpression-mediated migration, invasion and apoptosis of HTR-8 cells.

Hsa-miR-370-3p Inhibitor Suppressed Apoptosis and Enhanced Migration and Invasion of HTR-8 Cells

Next, we evaluated the functional role of hsa-miR-370-3p in FGR. As shown in Fig. 8A, the cells number of miR-370-3p inhibitor group that migrated to the bottom chamber was higher than that in the miR-NC inhibitor group. In the meantime, cells invasion showed the resemble results as migration. Finally, as shown in Fig. 8B, the percentage of apoptotic miR-370-3p inhibitor group cells was lower than in the miR-NC inhibitor group.

CDC25B is a Downstream Target of Hsa-miR-370-3p

Subsequently, we aimed to explore the mechanisms of hsa-miR-370-3p so we predicted the target mRNAs by online bioinformatics prediction on miRDB[30]. As shown in Supplementary Table S1, miRDB calculated with high context + score percentile and predicted 609 target mRNAs, among which 5 target mRNAs were candidate—GPRAB, PTPRB, CLOCK, FMR1 and CDC25B. Therefore, the 5 target mRNAs above were chosen to further identified. We first investigated the levels of these 5 target mRNAs in miR-370-3p-mimic, miR-NC, miR-370-3p-inhibitor and inhibitor-NC HTR-8 cells using qRT-PCR and western blots. We found that CDC25B expression was significantly lower in the miR-370-3p-mimic group than in the miR-NC group, while its expression was the higher in the miR-370-3p-inhibitor group than in the inhibitor-NC group.($P < 0.001$) (Fig. 9A, 9B), indicating that CDC25B might be the target mRNA of miR-370-3p.

Moreover, a dual luciferase activity assay was carried into execution to confirm the binding of hsa-miR-370-3p to linear CDC25B. As shown in Fig. 9C, the dual luciferase activity assay results showed that relative luciferase activity was clearly lower after hsa-miR-370-3p mimic transfection than after NC transfection, while relative luciferase activity was higher after hsa-miR-370-3p inhibitor transfection than after miR-NC inhibitor transfection. However, the mut-CDC25B transfection group was unable to come to the same results. It indicated that hsa-miR-370-3p mimic bound to the sequence of CDC25B cloned into

psi-CHECK2. Collectively, these data manifested that CDC25B acted as a downstream target for miR-370-3p in HTR-8 cells.

Discussion

Fetal growth restriction (FGR) is defined as a condition in which the fetus is fail to reach its potential for growth and development. The etiology of FGR is multifactorial, such as maternal causes, fetal causes, and causes involving placental insufficiency. Currently the incidence rates of FGR is the highest over the last decades and it is likely to grow, which becomes a public health challenge in both developed and developing countries[20]. As a newly discovered non-coding RNA, researchers all over the world pay great attention on circRNA. Nowadays, there are various methods which can be used to examine circRNA profiling, such as RT-qPCR, microarrays and NGS. Each method has its advantages and limitations; however, NGS have better sensitivity and capability of generating quantification. Neoteric bioinformatic approaches combined with biochemical enrichment strategies have allowed people to study circRNAs comprehensively, and many studies have proved circRNAs play an important role in human diseases[11]. Thousands of circRNAs have been identified as predictive biomarkers and have the potential to be therapeutic targets for therapy[21], [30]. Up to now, there are few reports on the relationship between circRNAs and FGR.

Maass et al. reported that some circRNAs of placenta might be related to pregnancy complications, such as fetal growth restriction, preeclampsia, HELLP syndrome, and diabetes[22]. Bai et al.[1]found some circRNAs, which were differentially expressed in placental tissue, contributed to the pathogenesis of preeclampsia. A placental villi circRNA screening from the Tang et al.[29] identified 55 upregulated circRNAs and 59 downregulated circRNAs between GDM patients and normal pregnancies. CircRNAs can be used as miRNA sponges to regulate genes expression. Wang et al.[29] provided hsa-circ-0000848 modulate the trophoblast cell function via the sponging of hsa-miR-370-3p. Nowadays, most studies of FGR focused on maternal causes. However, those placenta samples with maternal or fetal conditions leading to FGR were excluded from the study. According to our study, circRNAs may act as suitable biomarkers for uterine–placental perfusion, placental maldevelopment and insufficiency.

In this study, after all maternal and fetal causes were excluded from our samples, we characterized placenta-specific circRNAs in FGR. Firstly, by NGS, 18 placenta-specific circRNAs (hsa-circ-0005078, hsa-circ-0072697, hsa-circ-0084748, hsa-circ-0007440, hsa-circ-0005286, hsa-circ-0003288, hsa-circ-0035897, hsa-circ-0103279, hsa-circ-0005204, hsa-circ-0005939, hsa-circ-0006427, hsa-circ-0137008, hsa-circ-0006222, hsa-circ-0005238, hsa-circ-0088213, hsa-circ-0086190, hsa-circ-0002590, hsa-circ-0000972) were identified. Thus far, hsa-circ-0137008 was reported to suppress the malignant phenotype in colorectal cancer cells[33]. Other 17 circRNAs were reported for the first time.

Among the differentially expressed circRNAs in FGR, the qRT-PCR validation results of hsa-circ-0005238 attracted our attention. Hsa-circ-0005238 was notably decreased in the placentas of women with FGR, which has been not reported in pregnancy. Hence, we analyzed the functional role of hsa-circ-0005238 in

trophoblast cells by migration, invasion, and apoptosis analysis. Our results showed that hsa-circ-0005238 overexpression inhibited, while its knockdown promoted apoptosis in trophoblast cells. Moreover, hsa-circ-0005238 overexpression promoted, while its knockdown repressed cell migration and invasion in trophoblast cells. During the pregnancy, placental trophoblasts cells move upstream along the arterial wall, replace the endothelium, and disrupt the muscular lining[28]. Only then, the trophoblast invasion during human placentation enables fetus to derive nutrition from mater. Therefore, we conjectured that hsa-circ-0005238 may play an important role in the pathogenesis of FGR. Nevertheless, its mechanisms were needed to be confirm by further experiments.

Based on the regulatory model of circRNAs as microRNAs sponge, the inhibitory effect of miRNAs on the target genes then disappears, and the expression of the target gene enhanced. This process is referred to as the competitive endogenous RNA (ceRNA) mechanism[28]. Firstly, we predicted potential targets of hsa-circ-0005238 by bioinformatic analysis and identified hsa-miR-370-3p as a potential target miRNA of hsa-circ-0005238. MiR-370-3p was revealed as a tumor promoter in breast cancer[23] and gastric cancer[32]. It was pointed out that miR-370-3p was participate in fetal adrenal developmental programming[5]. However, how miR-370-3p are involved in FGR is unclear until now. Further, we found hsa-miR-370-3p was increased in the placentas of women with FGR. Moreover, hsa-circ-0005238 knockdown increased hsa-miR-370-3p expression in HTR-8 cells. Then hsa-circ-0005238 was confirmed as a sponge for hsa-miR-370-3p by luciferase reporter, AGO2 RIP assays and rescue experiment. MiRNAs inhibit target mRNA translation or participate in the degradation of target mRNA. In our work, hsa-miR-370-3p overexpression decreased CDC25B expression in HTR-8 cells. In addition, luciferase reporter proved CDC25B severd as a target mRNA for miR-370-3p in trophoblast cells. CDC25B is a member of phosphatases and key gene for entry into mitosis. When CDC25B is overexpressed, cells enter into mitosis before the usual time and show spindle abnormalities[17]. In contrast, depletion of CDC25B delays mitotic entry[17]. Lam[17] reported a unique Chinese girl who presented with intrauterine growth retardation as well as adolescent delayed development and she was diagnosed as homozygous non-sense variant in the CDC25B gene by whole-exome sequencing analysis. It is suggested that CDC25B may be potentially therapeutic for FGR. Regrettably, we did not make a profound study the downstream pathway of the hsa-circ-0005283/ miR-370-3p /CDC25B axis, which can be investigated in the future.

Conclusions

In summary, we demonstrate placenta-specific circRNAs in FGR pregnancy. Our data indicates that the downgraded expression of FGR placenta-specific hsa-circ-0005238 may take part in the occurrence and pathogenesis of FGR via decreasing CDC25B expression through sponging miR-370-3p. Our study also provides new insight into the molecular mechanism of FGR.

Abbreviations

FGR,fetal growth restriction; circRNAs, circular RNAs; NGS, next generation sequencing; GO,Gene Ontology; KEGG, Kyoto Encyclopedia of Genes and Genomes; qRT-PCR, quantitative real-time polymerase chain reaction; ncRNAs, non-coding RNAs; RIN, RNA integrity number; siRNA, small interfering RNA; BMI, body mass index

Declarations

Ethics approval and consent to participate

All methods were performed following the declaration of Helsinki ethical principles. This study was approved by the Medical Ethics Committee of Shenzhen Maternity and Child Healthcare Hospital ([2018]280). The patients/participants provided their written informed consent to participate in this study.

Consent for publication

Not Applicable

Availability of data and materials

All data generated or analysed during this study are included in this published article and its supplementary information files. RNA sequencing data analyzed in the article (Figure 1) have been deposited into CNGB Sequence Archive (CNSA)[14] of China National GeneBank DataBase (CNGBdb)[3] (https://db.cngb.org/cnsa/) with accession number CNP 0002703.

Competing interests

The authors declare that they have no competing interests.

Funding

Jilong Yao received a research grant from Science, Technology and Innovation Commission of Shenzhen Municipality (ZXSF201803).

Authors' contributions

ZH, QZ and JY conceived and designed the research. ZH performed the experiments; ZH and LZ analyzed the data; ZH, LZ and DZ prepared the figures and drafted the manuscript. ZH, QZ and JY edited and revised the manuscript.

Acknowledgements

Not applicable

References

1. Bai, Y, Rao, H, Chen, W, Luo, X, Tong, C, Qi, H Profiles of Circular RNAs in Human Placenta and their Potential Roles Related to Preeclampsia. *Biol Reprod* 2018;98:705-712.
2. Bu, D, Luo, H, Huo, P et al. KOBAS-i: Intelligent Prioritization and Exploratory Visualization of Biological Functions for Gene Enrichment Analysis. *Nucleic Acids Res* 2021;49:W317-W325.
3. Chen, FZ, You, LJ, Yang, F et al. CNGBdb: China National GeneBank DataBase. *Yi Chuan* 2020;42:799-809.
4. Chen, H, Zhang, Z, Feng, D Prediction and Interpretation of miRNA-disease Associations Based On miRNA Target Genes Using Canonical Correlation Analysis. *BMC Bioinformatics* 2019;20:404.
5. Chen, Y, Xia, X, Fang, M et al. Maternally Derived Low Glucocorticoid Mediates Adrenal Developmental Programming Alteration in Offspring Induced by Dexamethasone. *Sci Total Environ* 2021;797:149084.
6. Chowdhury, D, Choi, YE, Brault, ME Charity Begins at Home: Non-Coding RNA Functions in DNA Repair. *Nat Rev Mol Cell Biol* 2013;14:181-189.
7. Crispi, F, Figueras, F, Cruz-Lemini, M, Bartrons, J, Bijnens, B, Gratacos, E Cardiovascular Programming in Children Born Small for Gestational Age and Relationship with Prenatal Signs of Severity. *Am J Obstet Gynecol* 2012;207:121.
8. Crispi, F, Miranda, J, Gratacós, E Long-Term Cardiovascular Consequences of Fetal Growth Restriction: Biology, Clinical Implications, and Opportunities for Prevention of Adult Disease. *Am J Obstet Gynecol* 2018;218:S869-S879.
9. Darendeliler, F IUGR: Genetic Influences, Metabolic Problems, Environmental Associations/Triggers, Current and Future Management. *Best Pract Res Clin Endocrinol Metab* 2019;33:101260.
10. Esteller, M Non-Coding RNAs in Human Disease. *Nat Rev Genet* 2011;12:861-874.
11. Fang, X, Shrestha, SM, Ren, LH, Shi, RH Biological and Clinical Implications of Metastasis-Associated Circular RNAs in Oesophageal Squamous Cell Carcinoma. *FEBS Open Bio* 2021.
12. Fetal Growth Restriction: ACOG Practice Bulletin, Number 227 Fetal Growth Restriction: ACOG Practice Bulletin, Number 227. *Obstetrics & Gynecology* 2021;137.
13. Gong, S, Gaccioli, F, Dopierala, J et al. The RNA Landscape of the Human Placenta in Health and Disease. *Nat Commun* 2021;12:2639.
14. Guo, X, Chen, F, Gao, F et al. CNSA: A Data Repository for Archiving Omics Data. *Database (Oxford)* 2020;2020.
15. Hansen, TB, Jensen, TI, Clausen, BH et al. Natural RNA Circles Function as Efficient microRNA Sponges. *Nature* 2013;495:384-388.

16. Jeck, WR, Sorrentino, JA, Wang, K et al. Circular RNAs are Abundant, Conserved, and Associated with ALU Repeats. *RNA* 2013;19:141-157.
17. Karlsson, C, Katich, S, Hagting, A, Hoffmann, I, Pines, J Cdc25B and Cdc25C Differ Markedly in their Properties as Initiators of Mitosis. *J Cell Biol* 1999;146:573-584.
18. Kristensen, LS, Andersen, MS, Stagsted, L, Ebbesen, KK, Hansen, TB, Kjems, J The Biogenesis, Biology and Characterization of Circular RNAs. *Nat Rev Genet* 2019;20:675-691.
19. Lam, CW, Fong, NC, Chan, TY et al. Centrosome-Associated CDC25B is a Novel Disease-Causing Gene for a Syndrome with Cataracts, Dilated Cardiomyopathy, and Multiple Endocrinopathies. *Clin Chim Acta* 2020;504:81-87.
20. Lee, AC, Kozuki, N, Cousens, S et al. Estimates of Burden and Consequences of Infants Born Small for Gestational Age in Low and Middle Income Countries with INTERGROWTH-21(st) Standard: Analysis of CHERG Datasets. *BMJ* 2017;358:j3677.
21. Ma, Y, Zheng, L, Gao, Y, Zhang, W, Zhang, Q, Xu, Y A Comprehensive Overview of circRNAs: Emerging Biomarkers and Potential Therapeutics in Gynecological Cancers. *Front Cell Dev Biol* 2021;9:709512.
22. Maass, PG, Glažar, P, Memczak, S et al. A Map of Human Circular RNAs in Clinically Relevant Tissues. *J Mol Med (Berl)* 2017;95:1179-1189.
23. Mao, J, Wang, L, Wu, J et al. MiR-370-3p as a Novel Biomarker Promotes Breast Cancer Progression by Targeting FBLN5. *Stem Cells Int* 2021;2021:4649890.
24. Martins, JG, Biggio, JR, Abuhamad, A Society for Maternal-Fetal Medicine Consult Series #52: Diagnosis and Management of Fetal Growth Restriction: (Replaces Clinical Guideline Number 3, April 2012). *Am J Obstet Gynecol* 2020;223:B2-B17.
25. Nardozza, LM, Caetano, AC, Zamarian, AC et al. Fetal Growth Restriction: Current Knowledge. *Arch Gynecol Obstet* 2017;295:1061-1077.
26. Pels, A, Beune, IM, van Wassenaer-Leemhuis, AG, Limpens, J, Ganzevoort, W Early-Onset Fetal Growth Restriction: A Systematic Review On Mortality and Morbidity. *Acta Obstet Gynecol Scand* 2020;99:153-166.
27. Qu, S, Yang, X, Li, X et al. Circular RNA: A New Star of Noncoding RNAs. *Cancer Lett* 2015;365:141-148.
28. Sato, Y Endovascular Trophoblast and Spiral Artery Remodeling. *Mol Cell Endocrinol* 2020;503:110699.
29. Tang, L, Li, P, Li, L Whole Transcriptome Expression Profiles in Placenta Samples From Women with Gestational Diabetes Mellitus. *J Diabetes Investig* 2020;11:1307-1317.
30. van Zonneveld, AJ, Kölling, M, Bijkerk, R, Lorenzen, JM Circular RNAs in Kidney Disease and Cancer. *Nat Rev Nephrol* 2021.
31. Wang, H, Zhang, J, Xu, Z et al. Circular RNA Hsa_Circ_0000848 Promotes Trophoblast Cell Migration and Invasion and Inhibits Cell Apoptosis by Sponging hsa-miR-6768-5p. *Front Cell Dev Biol* 2020;8:278.

32. Yang, J, Zhang, X, Cao, J et al. Circular RNA UBE2Q2 Promotes Malignant Progression of Gastric Cancer by Regulating Signal Transducer and Activator of Transcription 3-Mediated Autophagy and Glycolysis. *Cell Death Dis* 2021;12:910.
33. Yang, Z, Zhang, J, Lu, D et al. Hsa_Circ_0137008 Suppresses the Malignant Phenotype in Colorectal Cancer by Acting as a microRNA-338-5p Sponge. *Cancer Cell Int* 2020;20:67.
34. Zhang, XO, Dong, R, Zhang, Y et al. Diverse Alternative Back-Splicing and Alternative Splicing Landscape of Circular RNAs. *Genome Res* 2016;26:1277-1287.

Figures

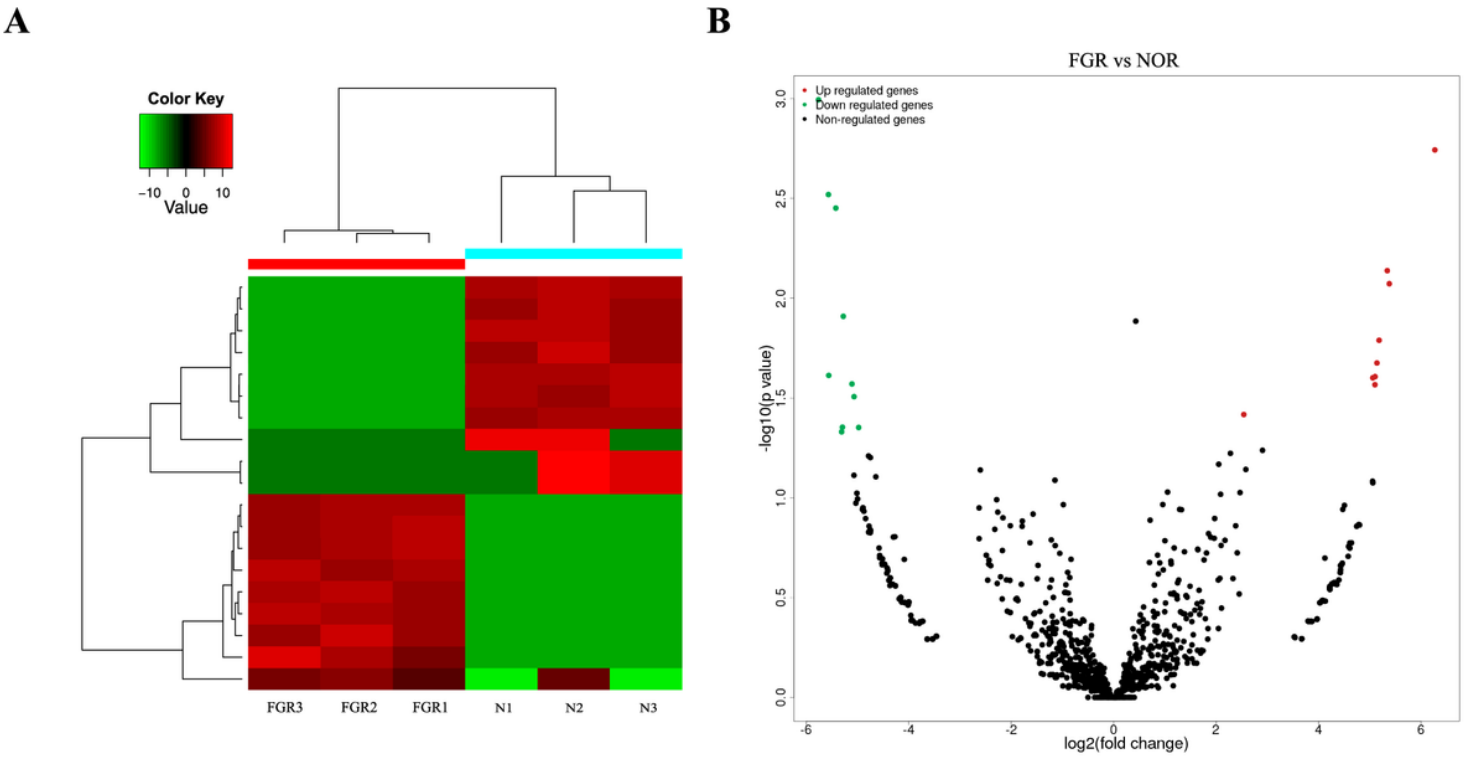

Figure 1

Bioinformatic analysis of the results of circRNA. (A) Heatmap of differentially expressed circRNAs in FGR vs Normal samples (N). The heatmap shows a distinguishable circRNA expression profile between groups. Black: no change; red: upregulation; green: down-regulation. (B) Volcano plots of differentially expressed circRNAs between groups (N). Red point: up-regulated CircRNAs after applying |log2FC| ≥1; green point: down-regulated CircRNAs after applying |log2FC| ≥1.

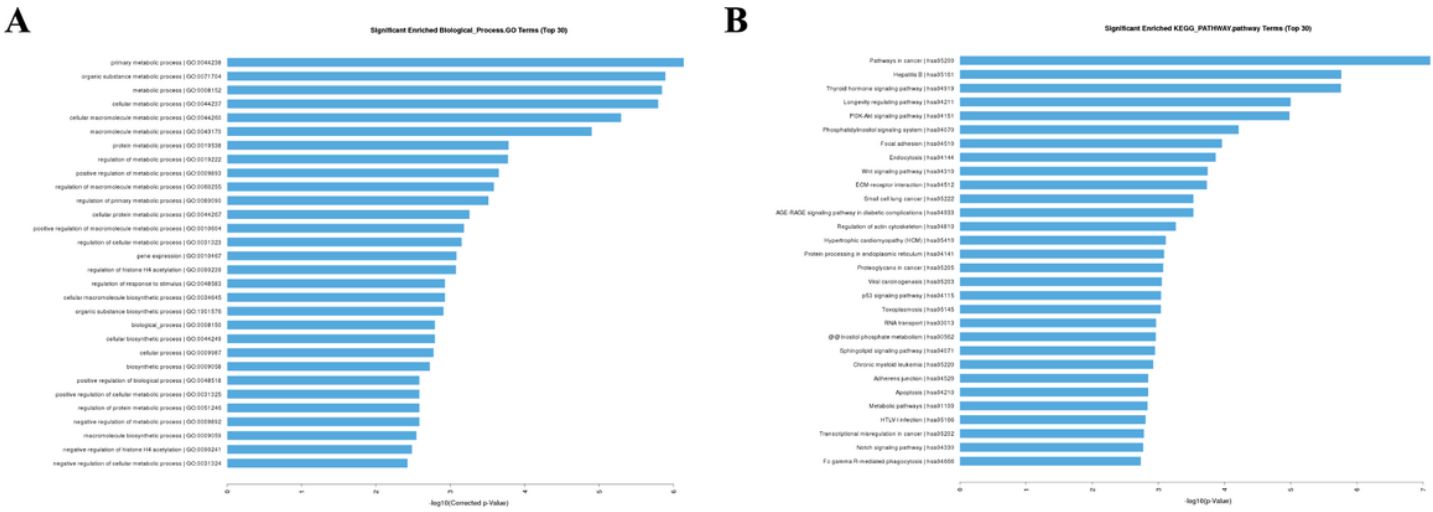

Figure 2

GO and KEGG enrichment analysis. (A) Top 30 classes of biological process enrichment terms. (B) Top 30 classes of KEGG pathway terms.

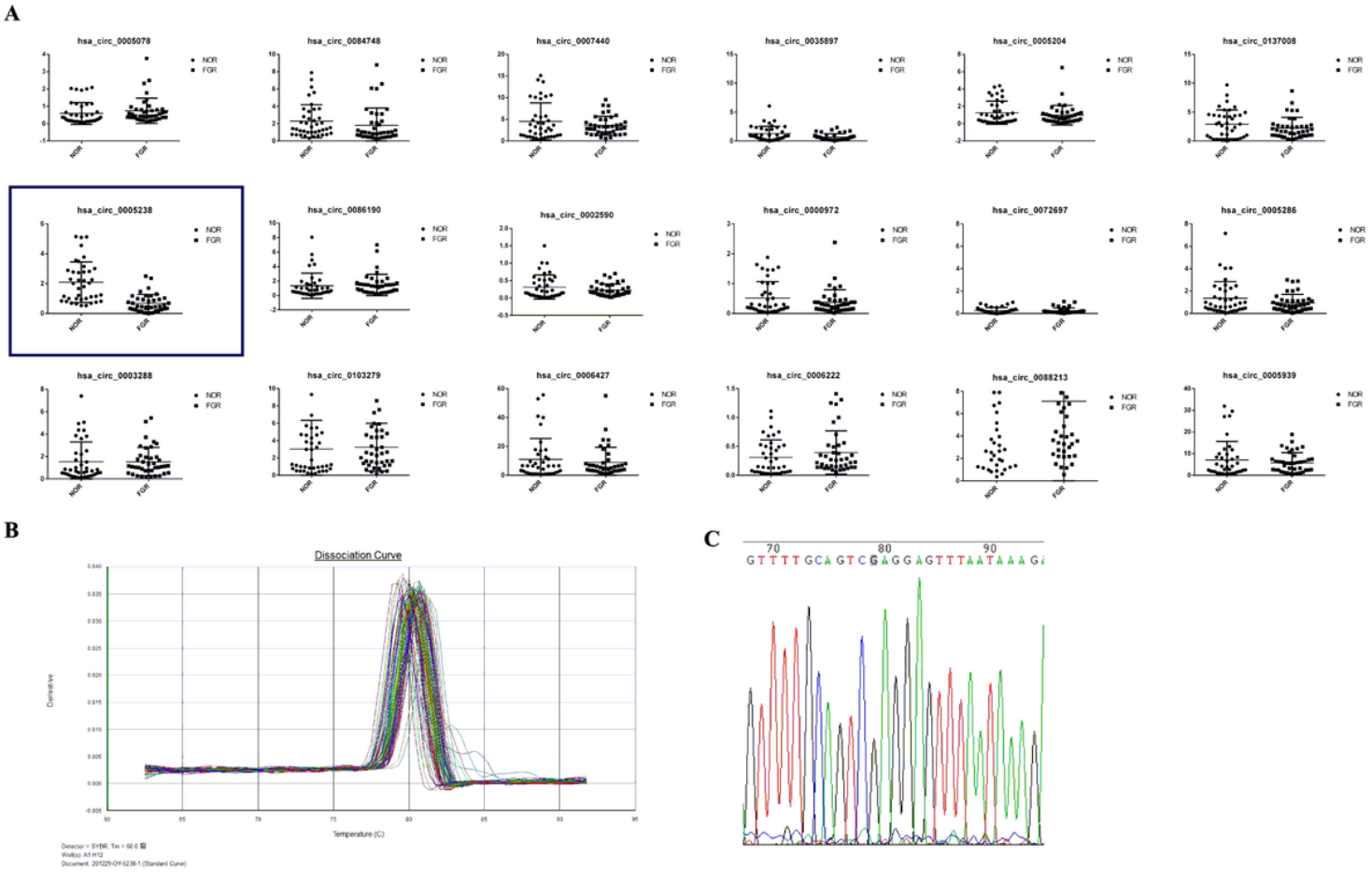

Figure 3

qRT-PCR verification of 18 differentially expressed circRNAs. (A) The expression profiles of 18 differentially expressed circRNAs by RT-PCR were consistent with the NGS results. Hsa-circ-0005238 was displayed in the blue box, which was significantly downregulation in FGR group. (B) Melting curve analysis of hsa-circ-0005238. (C) Sequencing analysis around the splice junction of hsa-circ-0005238 fragment in RT-qPCR.

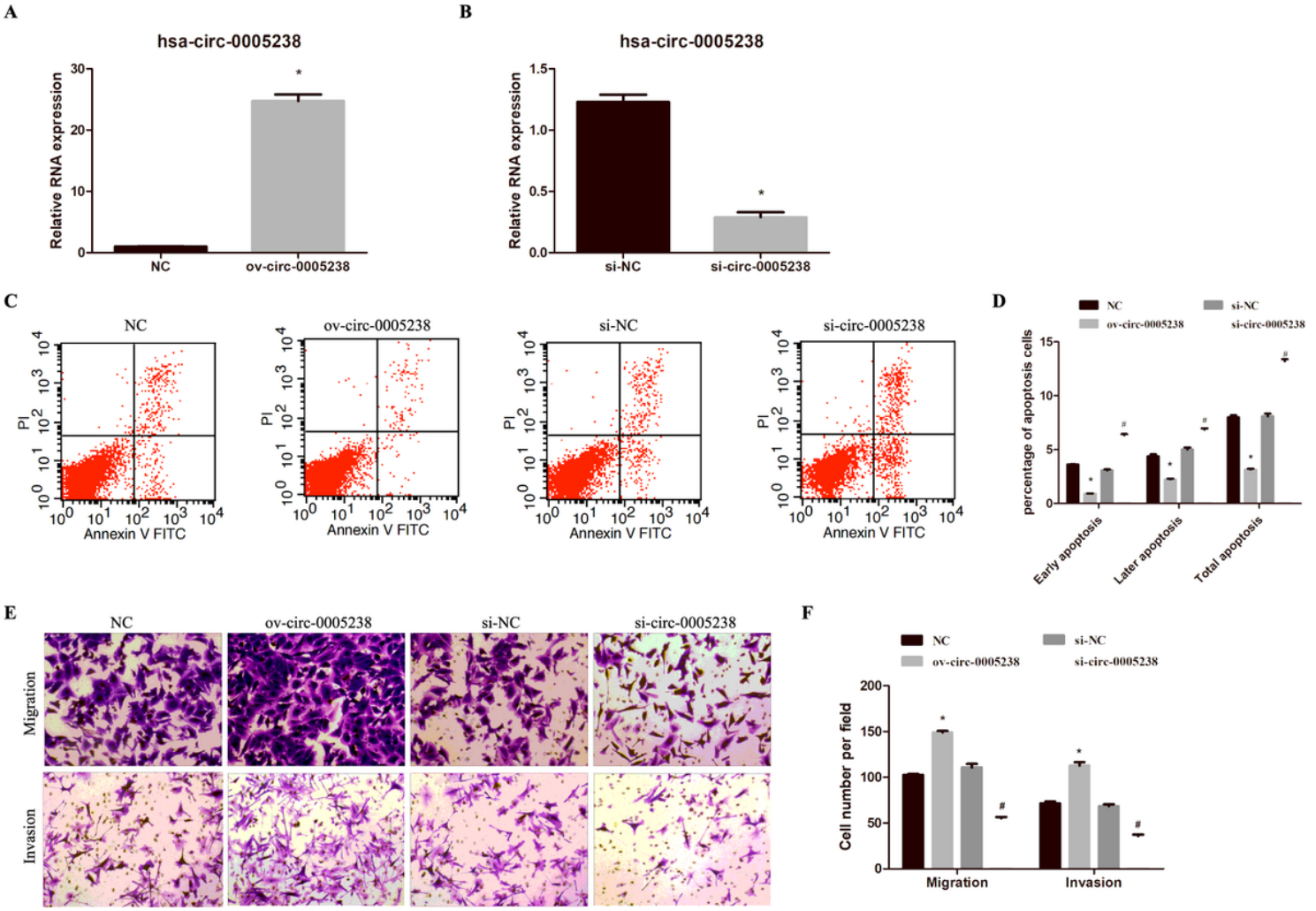

Figure 4

Effect of hsa-circ-0005238 overexpression or knockdown on biological functions of HTR-8 cells. (A) Hsa-circ-0005238 is overexpressed in HTR-8 cells after transfection with hsa-circ-0005238 containing plasmid (ov-circ-0005238) compared to negative control plasmid (NC). (B) Hsa-circ-0005238 expression is lower in HTR-8 cells after transfection with siRNA targeting hsa-circ-0005238 (si-circ-0005238) compared to that in NC siRNA (si-NC). (C, D) Effect of hsa-circ-0005238 overexpression or knockdown on the apoptosis of HTR-8 cells. Panel C shows representative graphs of the apoptosis detected using a flow cytometer. Panel D shows quantification of the percentage of apoptotic cells. (E, F) Effect of hsa-circ-0005238 overexpression or knockdown on the migration and invasion of HTR-8 cells. Panel E representative images of migration and invasion by Transwell assay and Boyden assay. Panel F includes bar graphs representing the quantification of migrated or invaded cell numbers.

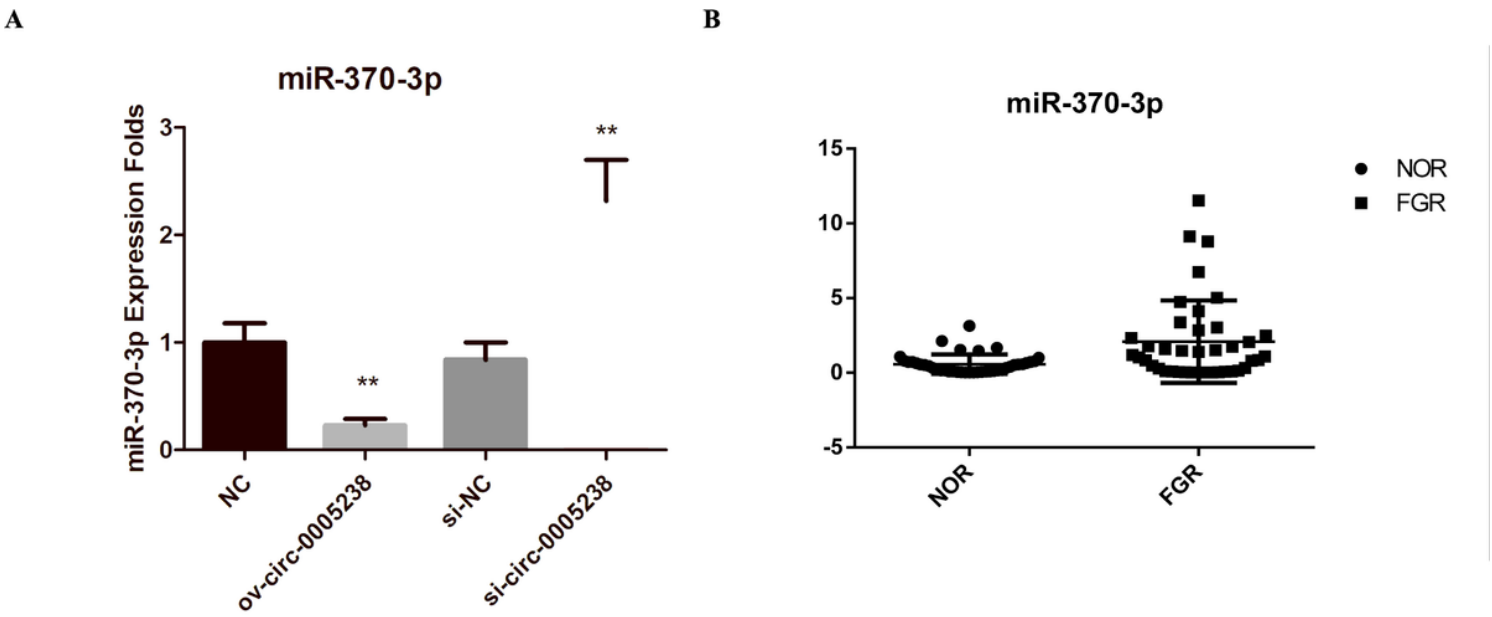

Figure 5

Expression of hsa-miR-370-3p in the ov-circ-0005283, si-circ-0005283 group and FGR placenta. (A) Expression of miR-370-3p in ov-circ-0005283, ov-NC, si-circ-0005283 and si-NC group. (B) hsa-miR-370-3p expression in FGR or normal placental tissues (n = 40).

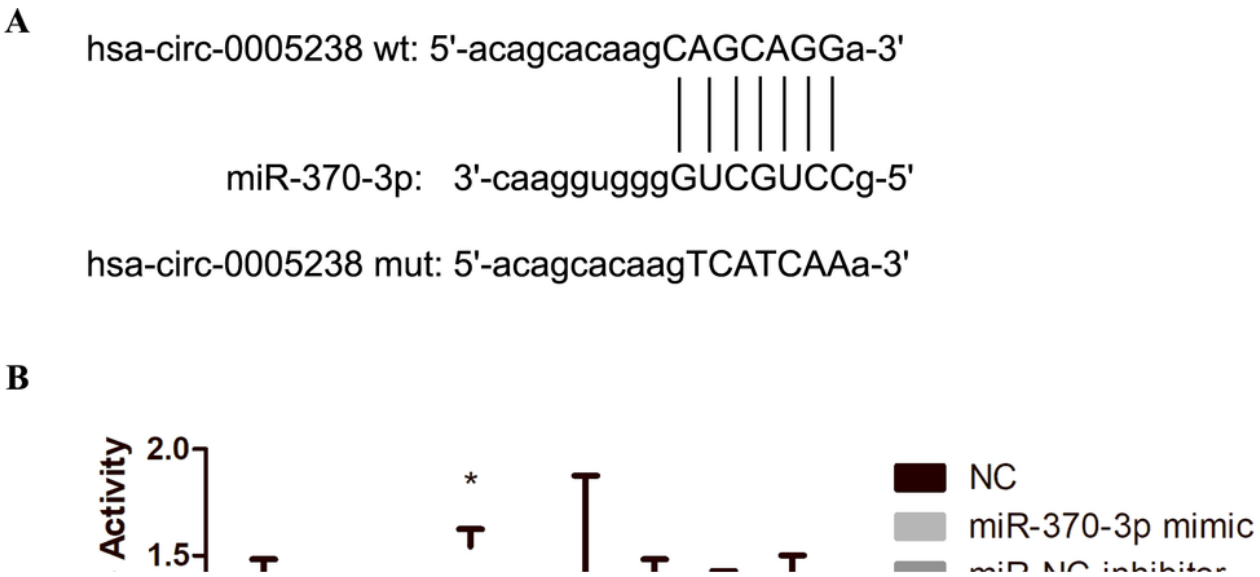

Figure 6

hsa-miR-370-3p was targeted by hsa-circ-0005283 in HTR-8 cells. (A) The binding site of hsa-miR-370-3p on hsa-circ-0005283 and the mutant information for hsa-circ-0005283 in the dual luciferase activity assay. (B) Results of the dual luciferase activity assay. (C) Results of the anti-AGO2 immunoprecipitation (RIP) assay.

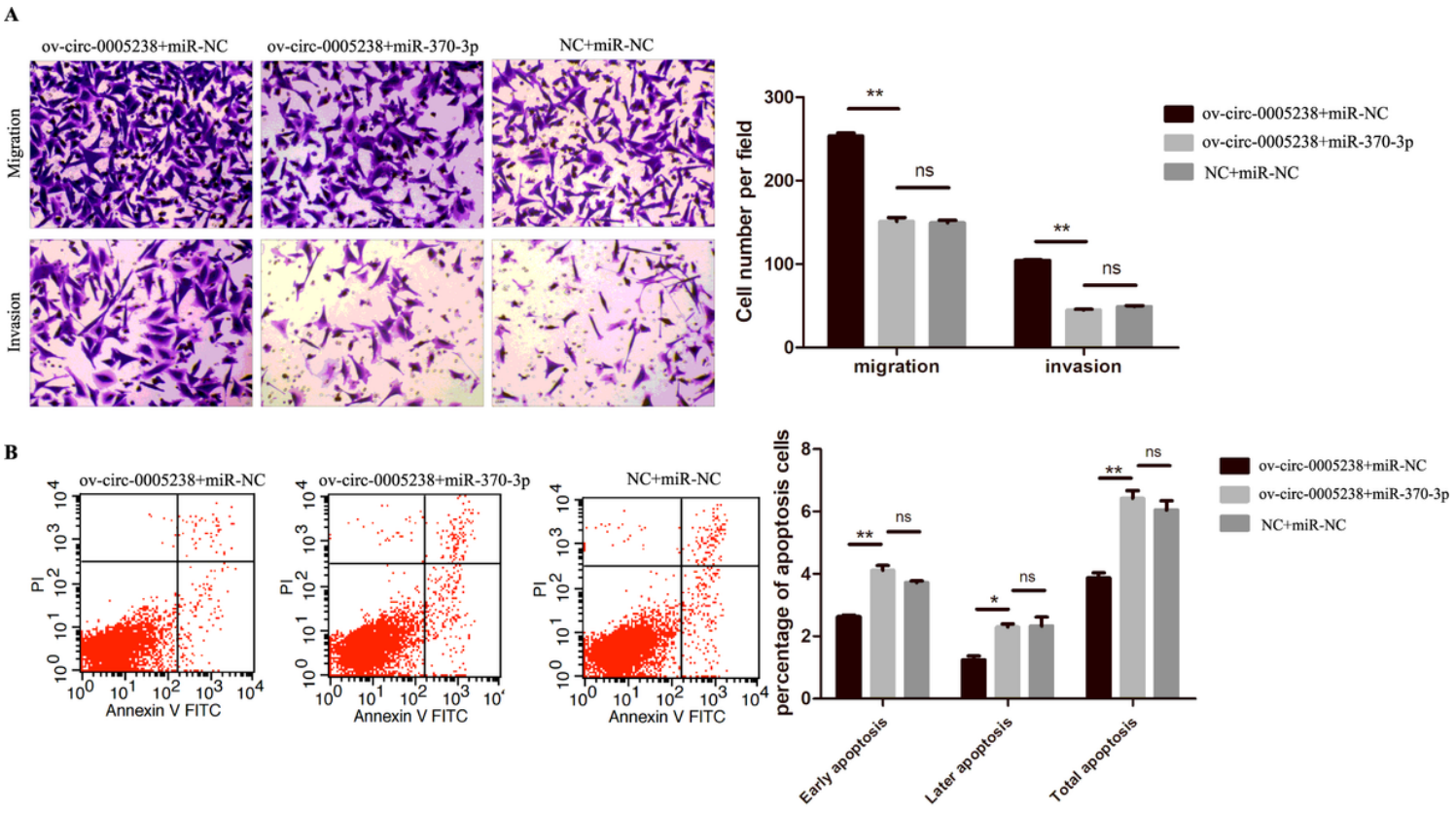

Figure 7

hsa-miR-370-3p overexpression eliminated the effect of hsa-circ-0005283 overexpression in HTR-8 cells. (A) The left panel includes representative images of migration and invasion. The right panel includes bar graphs of the quantification of migrated or invaded cell numbers. (B) The left panel shows quantification of the percentage of apoptotic cells. The right panel shows representative graphs of the apoptosis detected using a flow cytometer.

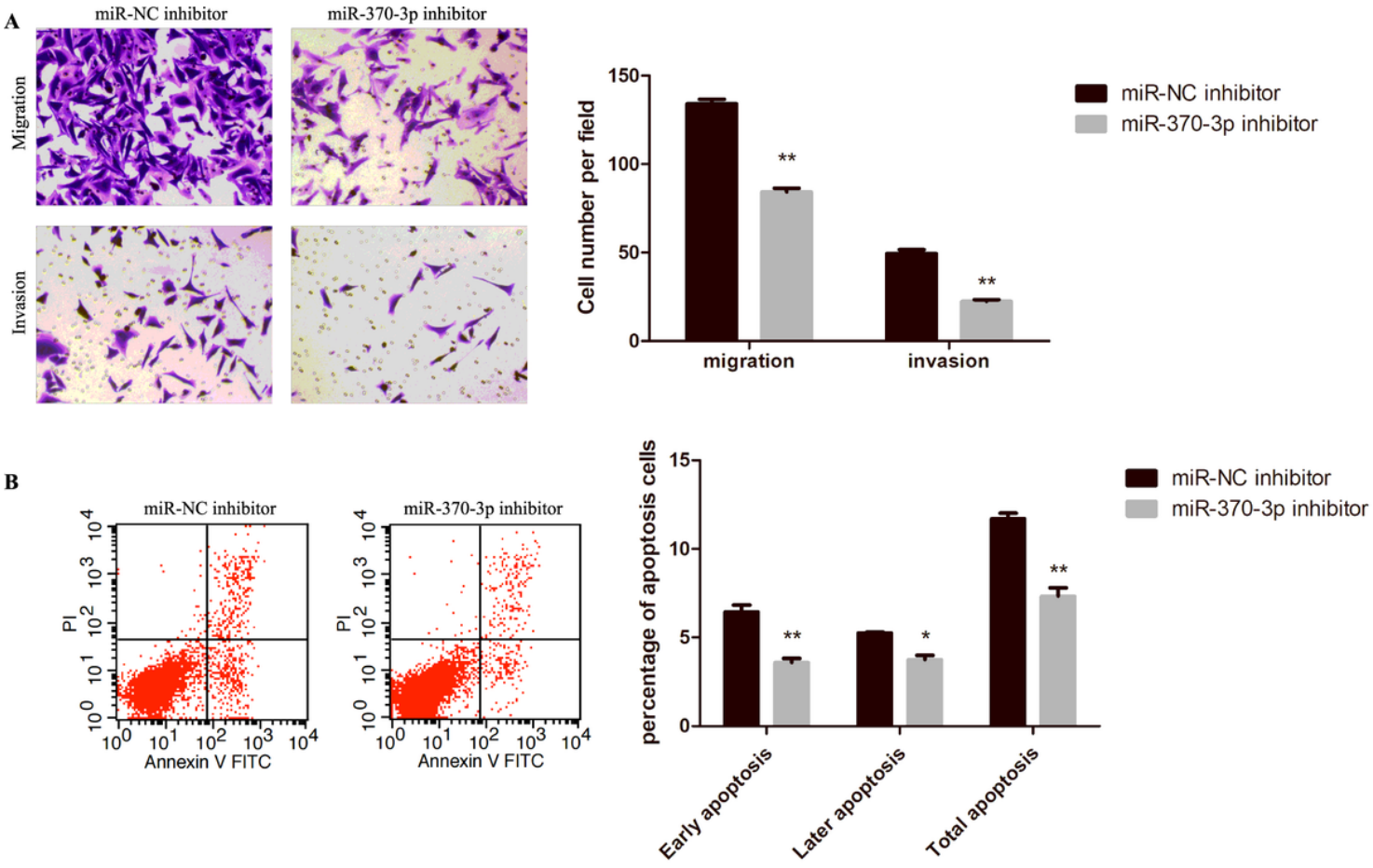

Figure 8

Effect of hsa-miR-370-3p knockdown on apoptosis, migration and invasion of HTR-8 cells. (A) The left panel includes representative images of migration and invasion. The right panel includes bar graphs of the quantification of migrated or invaded cell numbers. (B) The left panel shows quantification of the percentage of apoptotic cells. The right panel shows representative graphs of the apoptosis detected using a flow cytometer.

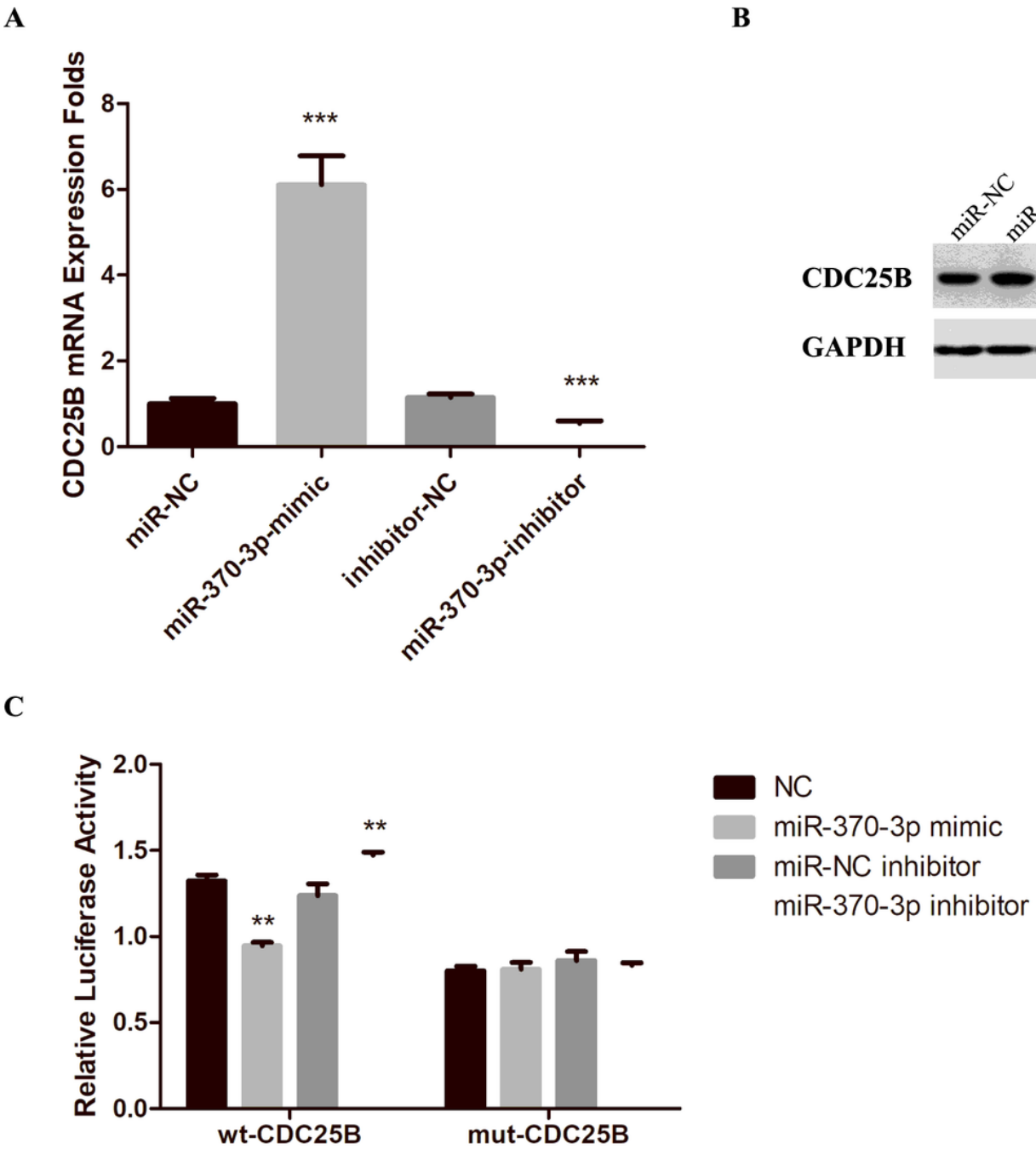

Figure 9

CDC25B is a direct target of miR-370-3p. (A) Expression of CDC25B in miR-370-3p-mimic, miR-NC, inhibitor- miR-370-3p and inhibitor-NC group by RT-qPCR. (B) Western Blot results of CDC25B expression in miR-370-3p-mimic, miR-NC, inhibitor- miR-370-3p and inhibitor-NC group. (C) Results of the dual luciferase activity assay.

Supplementary Files

This is a list of supplementary files associated with this preprint. Click to download.

- SupplementaryTableS1predictthetargetmRNAsofhsamiR3703p.pdf
- fulllengthblotsCDC25B.pdf
- fulllengthblotsGAPDH.pdf